Frontiers in Marine Science

TYPE Original Research
PUBLISHED 02 July 2025
DOI 10.3389/fmars.2025.1619142

Role of wind stress directional steadiness in modulating mesoscale air-sea interactions in the Western Arabian Sea

Xingyu Liu[1], Sana Ben Ismail[2] and Yuntao Wang[1*]

[1]South China Sea Institute of Oceanology, Hangzhou, China, [2]Laboratory Milieu Marin, Institute National des Sciences et Technologies de la Mer, Tunis, Tunisia

OPEN ACCESS

EDITED BY
Meilin Wu,
Chinese Academy of Sciences (CAS), China

REVIEWED BY
Jinglong Yao,
Chinese Academy of Sciences (CAS), China
Anil Akpinar,
Middle East Technical University, Türkiye

*CORRESPONDENCE
Yuntao Wang
yuntao.wang@sio.org.cn

RECEIVED 27 April 2025
ACCEPTED 04 June 2025
PUBLISHED 02 July 2025

CITATION
Liu X, Ben Ismail S and Wang Y (2025) Role of wind stress directional steadiness in modulating mesoscale air-sea interactions in the Western Arabian Sea. *Front. Mar. Sci.* 12:1619142. doi: 10.3389/fmars.2025.1619142

Mesoscale air-sea interactions reveal the dependence between wind stress and sea surface temperature (SST) where the wind stress directional steadiness (WSDS) serves as a critical role in modulating such interaction. Using satellite-derived SST and reanalysis wind stress data (2003–2022), this study investigates WSDS-mediated coupling in the western Arabian Sea, demonstrating that during the summer monsoon, persistently high WSDS creates optimal conditions for air-sea interactions. The coupling coefficients between wind stress curl (WSC) and crosswind SST gradient (CWSG) exhibits a monotonic strengthening from May ($r = 0.80$) to September ($r = 0.93$), with prolonged high WSDS enhancing coupling coefficients through cumulative effects. This intense coupling arises from southwest monsoon-driven coastal upwelling that generates sharp SST fronts. In contrast, the winter monsoon lacks upwelling and frontal activity, suppressing the interactions. Transitional seasons exhibit intermediate behavior that spring shows strengthening coupling as WSDS increases with monsoon onset, while autumn exhibits diminishing coupling as WSDS declines post-monsoon. These results highlight WSDS as a key regulator of mesoscale air-sea interactions in monsoon-dominated regions.

KEYWORDS

wind stress directional steadiness, mesoscale air-sea interactions, front, upwelling, coupling coefficient, Arabian Sea

1 Introduction

The relationship between sea surface temperature (SST) and wind stress has been widely used to characterize regional air-sea coupling, with distinct dependence emerging across spatiotemporal scales and geographic regions (Chelton et al., 2004; Xie, 2004; Small et al., 2008; O'Neill, 2012). At large scales (>1,000 km), atmospheric forcing dominates ocean variability, producing a negative SST-wind stress coupling primarily through wind-driven evaporation and latent heat release (Frankignoul and Hasselmann, 1977; Czaja and Frankignoul, 2002). This mechanism is particularly evident in the extratropic, where stochastic atmospheric forcing overwhelms oceanic feedbacks (Deser et al., 2010). At small scales (1–10 km), localized air-sea exchanges are influenced by surface waves (Sullivan and McWilliams, 2010), temperature gradients, and salinity variations. These interactions induce rapid (hourly to daily) modifications in boundary layer stability through turbulent mixing, predominantly affecting near-surface wind patterns (Gaube et al., 2015; Wenegrat and Arthur, 2018). However, their vertical influence is generally confined within the marine boundary layer, with limited horizontal extent. In contrast, mesoscale interactions (10–100 km) exhibit more persistent and systematic ocean-atmosphere coupling. Sustained SST anomalies associated with oceanic fronts and eddies reorganize boundary layer structure via thermodynamic adjustment processes over weekly to monthly timescales (Chelton et al., 2007; Frenger et al., 2015). These mesoscale features generate secondary circulations that significantly alter wind stress patterns (Cui et al., 2020) and can vertically propagate to influence free atmospheric processes, including cloud formation and precipitation. Horizontally, the impact of mesoscale SST anomalies can extend over hundreds of kilometers, creating coherent atmospheric responses. For instance, observational studies in the North Atlantic (Bryan et al., 2010), Gulf Stream (Park and Cornillon, 2002), and equatorial Pacific (Hayes et al., 1989) have demonstrated that winds blowing from colder to warmer SST regions enhance surface stress and heat fluxes (Wallace et al., 1989). Similar coupling patterns have been observed in the Antarctic Circumpolar Current (Frenger et al., 2013) and western boundary currents (Ma et al., 2016), highlighting the ubiquity of mesoscale air-sea feedbacks in dynamically active regions (Chelton et al., 2004; O'Neill et al., 2010; O'Neill, 2012).

Mesoscale air-sea interaction is a critical process governing the exchange of material and energy between the ocean and atmosphere (Small et al., 2008; Chelton and Xie, 2010), serving as a fundamental driver of variability in oceanic and atmospheric circulations (O'Reilly and Czaja, 2015; Ma et al., 2017). The ocean and atmosphere continuously exchange momentum, heat, and mass, with surface wind stress, thermal fluxes, and momentum fluxes playing pivotal roles in driving surface currents and redistributing heat across the global ocean (Bourassa et al., 2013; Cronin et al., 2019). Conversely, atmospheric responses to mesoscale SST anomalies feed back onto the ocean by modulating wind-driven mixing and upwelling, thereby influencing ocean circulation patterns (Chelton and Xie, 2010). The upper-ocean mixed layer acts as a critical mediator of these exchanges, with SST and wind stress emerging as key variables that reflect both thermal and dynamic coupling (Sun et al., 2020). Given their central role in regulating global climate and ocean circulation (Yu et al., 2020), accurately representing mesoscale air-sea interactions are essential for improving numerical predictions of weather and climate (Chen et al., 2022).

Mesoscale SST-wind stress coupling is most pronounced near oceanic fronts, where cross-frontal SST gradients induce atmospheric boundary layer (ABL) instability. This instability enhances vertical momentum mixing and increases surface wind stress over warmer waters, deepening the ABL and facilitating the downward transfer of momentum from the free atmosphere to the ocean surface, thereby accelerating surface winds (Small et al., 2008; Chelton and Xie, 2010; O'Neill et al., 2010). In contrast, colder waters stabilize the ABL and suppress near-surface winds (Chelton and Xie, 2010). As a result, a positive coupling coefficient between SST and wind stress is predominantly observed in frontal regions of the global ocean (Chelton et al., 2004). This coupling mechanism further generates wind stress curl (WSC) anomalies that are approximately proportional to crosswind SST gradients (CWSG) within frontal zones (Chelton et al., 2001; see Equations 1–3). Coupling coefficients, defined as the regression slope between WSC and CWSG, are commonly used to quantify the strength of the interaction (O'Neill et al., 2010). Observations consistently reveal substantial spatial variability in coupling coefficients across the global ocean (Wang and Castelao, 2016).

A critical factor modulating mesoscale SST-wind stress coupling is wind stress directional steadiness (WSDS), defined as the ratio of vector-averaged to scalar-averaged wind speed, which reflects the directional stability of surface winds (Chelton et al., 2007; see Equation 4). High WSDS, indicating stable wind directions, enhances SST-wind stress coupling by allowing the ABL to respond more consistently to underlying SST gradients (Chelton et al., 2001; Xie, 2004; Small et al., 2008). For instance, in the Brazil Current region, coupling coefficient is low during the onset of the monsoon but increases substantially as WSDS elevates (Castelao, 2012). Seasonal variations in WSDS have therefore been shown to drive pronounced intra-annual changes in mesoscale coupling intensity (Sun et al., 2020; Yu et al., 2020). In monsoon-dominated systems such as the Arabian Sea, the summer southwest monsoon induces strong coastal upwelling along the coasts of Oman and Somalia (Schott et al., 2009), generating prominent SST fronts that modulate surface winds (Vecchi et al., 2004; Xie, 2004). In contrast, the winter northeast monsoon is less favorable for frontogenesis and associated with weaker mesoscale air-sea interactions (Beal and Donohue, 2013).

Prior studies have elucidated key mechanisms governing mesoscale SST-wind stress coupling, including vertical momentum mixing, pressure adjustments, and WSDS (Chelton et al., 2004; Small et al., 2008; Castelao, 2012). Vertical momentum mixing refers to the turbulent exchange of momentum between the ocean surface and the ABL (Wallace et al., 1989; Hayes et al., 1989), which influences the intensity of the wind stress acting on the sea surface. This process can modify the feedback between SST and wind stress by altering the vertical profiles of velocity and turbulence (Small et al., 2003). Pressure adjustments involve SST anomalies induced changes in atmospheric pressure fields that can modulate wind patterns by adjusting the local pressure gradient force, thus affecting the strength and direction of wind stress near the ocean surface (Chelton and Xie, 2010). WSDS refers to the temporal variability of wind direction, which affects the development of air-sea coupling. When wind direction changes rapidly, the ocean has insufficient time to respond fully to atmospheric forcing, disrupting the coupling process (Chelton et al., 2004; Small et al., 2008). Conversely, more stable wind directions provide the necessary time for effective ocean-atmosphere interactions, thereby enhancing the strength of the coupling. Despite these advancements, substantial uncertainties persist in accurately quantifying mesoscale air-sea coupling and assessing its impacts on ocean dynamics (Chelton and Xie, 2010; Frenger et al., 2013). In particular, the impacts of vertical momentum mixing and pressure adjustments have been well investigated in former studies; however, the quantitative role of WSDS in modulating mesoscale air-sea interactions remains poorly understood, and the temporal evolution of these interactions requires further investigation. It is crucial to evaluate the influences of WSDS on the intensity, temporal evolution, and spatial variability of the coupling between wind stress and SST gradients, especially under the complex seasonal monsoon forcing and upwelling dynamics. The western Arabian Sea, characterized by strong seasonal monsoon variability (Schott et al., 2009), provides an ideal natural laboratory to investigate these processes.

In this study, we systematically evaluate mesoscale SST-wind stress coupling by synthesizing satellite observations and reanalysis products, with a particular focus on coastal frontal regions. We investigate the role of WSDS on modulating coupling strength, following observational frameworks established in recent studies (e.g., Oerder et al., 2016; Shao et al., 2019; Cui et al., 2020), which demonstrated that mesoscale SST gradients can substantially reshape surface wind stress patterns through ABL adjustments, with the degree of coupling strongly influenced by wind persistence and stability. Building on these insights, our findings aim to advance the understanding of mesoscale processes that are critical for marine ecosystem dynamics, regional climate resilience, and the predictability of the coupled Earth system.

2 Data and methods

The SST data are derived from the Moderate Resolution Imaging Spectroradiometer (MODIS), developed by NASA. MODIS provide data across 36 spectral bands ranging from 0.4 μm to 14.4 μm at different spatial resolutions (2 bands at 250 m, 5 bands at 500 m, and 29 bands at 1 km). It provides daily measurements with spatial resolution of 4km (Kilpatrick et al., 2015). The data is sensitive to provide measurements of mesoscale to large-scale global dynamics, aiding in the tracking of variability over time (Barnes and Salomonson, 1995). The time range of the data is 20 years from January 2003 to December 2022, covering a complete 20-year period that captures multiple annual cycles.

The wind stress data are sourced from the fifth-generation atmospheric reanalysis dataset ERA5, produced by the European Centre for Medium-Range Weather Forecasts (ECMWF) for global climate from January 1950 to the present. ERA5 represents nearly 80 years of ECMWF's reanalysis of global climate and weather. This study utilizes daily averaged reanalysis data spanning from January 2003 to December 2022, consistent with SST dataset. The data are organized into a regular grid with a resolution of 0.25 degrees (Hersbach et al., 2020). To ensure spatial consistency, the original high-resolution SST data (4 km × 4 km) were interpolated to match the ERA5 wind field resolution (0.25° × 0.25°) using bilinear interpolation. This standardized grid system preserves the physical relationships between oceanic and atmospheric variables while enabling accurate calculation of CWSG relative to wind direction. The bilinear interpolation method effectively maintains both the magnitude and directional characteristics of SST gradients, which are crucial for robust air-sea interaction analysis.

WSC quantifies the rotational effect of wind stress on the ocean surface, indicating the tendency of the wind to induce cyclonic or anticyclonic circulation in the upper ocean. CWSG is the component of the SST gradient that runs perpendicular to the direction of wind. It reflects lateral variations in temperature across wind. The CWSG and WSC are calculated based on the method outlined by Wang and Castelao (2016):

$$\mathbf{WSC}=\frac{\partial\tau_y}{\partial x}-\frac{\partial\tau_x}{\partial y} \tag{1}$$

τ_x and τ_y represent the zonal (eastward) and meridional (northward) components of wind stress, respectively, $\frac{\partial}{\partial x}$ and $\frac{\partial}{\partial y}$ denote the partial derivatives along longitude and latitude directions.

$$\nabla \mathbf{T} = \left(\frac{\partial \mathbf{T}}{\partial x}, \frac{\partial \mathbf{T}}{\partial y}\right) \tag{2}$$

$$\mathbf{CWSG} = \nabla \mathbf{T} \times \hat{\boldsymbol{\tau}} \tag{3}$$

where ∇T is the SST gradient, $\frac{\partial T}{\partial x}$ is the zonal (east-west) component of SST gradient, $\frac{\partial T}{\partial y}$ is the meridional (north-south) component of SST gradient. $\hat{\tau}$ is the unit vector of wind stress direction, $\times$ denotes the cross product.

WSDS is calculated as the ratio between the vector-averaged wind stress and magnitude-averaged wind stress (Bryan et al., 2010; O'Neill, 2012).

$$\mathbf{WSDS} = \frac{|\langle\vec{\tau}\rangle|}{\langle|\vec{\tau}|\rangle} \tag{4}$$

Where $\vec{\tau} = (\tau_x, \tau_y)$ is the wind stress vector, with τ_x and τ_y representing the zonal (eastward) and meridional (northward) components, respectively. $|\langle\vec{\tau}\rangle| = \sqrt{\langle\tau_x\rangle^2+\langle\tau_y\rangle^2}$ is the magnitude of the vector-averaged wind stress. The angle brackets $\langle\cdot\rangle$ denote a vector average (time or spatial mean) of the wind stress components τ_x and τ_y. $\langle|\vec{\tau}|\rangle = \left\langle\sqrt{\tau_x^2+\tau_y^2}\right\rangle$ is the magnitude-averaged wind stress (time or spatial mean). The normalized value of WSDS constrains a value within the range of [0, 1], and thereby quantifying the directional variability relative to the overall wind stress magnitude. Specifically, when the wind stress is consistently oriented in a single direction over time, the wind vector is reinforced each other, i.e., with high WSDS approaching 1. In contrast, if the wind direction fluctuates significantly, the vector averaging causes partial cancellation among components, reducing $|\langle\vec{\tau}\rangle|$ and indicating greater directional dispersion with WSDS approaching 0 (O'Neill, 2012).

All variables were averaged over 29-day periods at 7-day intervals, following the methodology commonly used in mesoscale air-sea interaction studies, to capture subseasonal variability while smoothing out high-frequency noise (e.g., Bryan et al., 2010; O'Neill, 2012). This temporal averaging scheme effectively isolates the ocean-atmosphere coupling signals associated with mesoscale eddies and fronts, as shorter periods may retain synoptic weather influences, whereas longer periods could obscure transient coupling dynamics (Chelton and Xie, 2010). All data were processed as anomalies by removing climatological means, thereby effectively isolating mesoscale signals from seasonal cycles and long-term trends, in consistent with standard procedures from former studies (Gaube et al., 2015).

Mesoscale air-sea coupling strength is quantified through a coupling coefficient combining binned averaging and linear regression techniques between CWSG and WSC (Gaube et al., 2015). This method captures the thermodynamic forcing of mesoscale ocean features on the ABL, where positive regression coefficients indicate that SST-induced pressure gradients elevate the spatial variation in wind stress that high SST is associated with high wind stress (Chelton and Xie, 2010; Renault et al., 2019). The coefficient with values being seasonally dependent due to variations in background wind fields (Small et al., 2008; Wikle, 2015).

3 Results

3.1 Climatological patterns of Western Arabian Sea upwelling and air-sea coupling

The western Arabian Sea exhibits significant variations in water depth, transitioning from shallow continental shelf areas to deep-sea basins exceeding 4,000 meters. The continental shelves along the Oman coastline are relatively narrow, with water depths exceeding 2,000 meters within a short offshore distance. The Somalia upwelling region lies over the relatively shallow continental slope and shelf, where depths range from a few hundred meters near the coast to approximately 1,000–1,500 meters over the shelf, before descending sharply into the deep-sea zone (Figure 1a).

Averaged SST and wind stress in the western Arabian Sea exhibit a monotonic increase from coastal zones to the open ocean (Figure 1b). Two prominent cold-water anomalies are observed, i.e., a primary core near the coast of Somalia (4°N–10°N) and a secondary zone off Oman (17°N–20°N). Along the Somalia shelf, horizontal SST gradients exceed 7°C per 100 km. As monsoon winds pass over regions with contrasting SST, spatial variations in vertical turbulent mixing enhance (suppress) wind stress over warm (cooler upwelled) waters, thereby modulating the near-surface wind field (Chelton et al., 2007). This air-sea coupling (Figure 1b) is exemplified in the Somalia upwelling region (6°N–11°N) with tight coupling among parallel wind stress vectors (>0.2 N/m²) and steep SST gradients (>4°C per 100 km), underscoring the importance of Ekman-driven offshore transport induced self-reinforcing feedback loop (Wang et al., 2021). The resultant cold upwelling plume, confined to a narrow coastal strip (<100 km), sharply attenuates seaward due to opposing influences from the warm western Arabian Sea Current (SST >28°C) and turbulent dissipation. Notably, the Oman upwelling zone (20°N–25°N) is characterized by broader but weaker SST gradients (Figure 1b; 2–3°C per 100 km). In contrast, the central western Arabian Sea shows consistently weaker SST gradients (<1°C per 100 km), spatially coinciding with wind stress convergence zones (Figure 1b).

Multi-year averaged SST gradient and wind stress reveal robust spatiotemporal coupling coefficients between CWSG and WSC across the western Arabian Sea. The results demonstrate strong spatial coherence between WSC and CWSG in the Somalia coastal upwelling region, with significantly positive coupling coefficients (Figure 1c). The nearshore CWSG values 2°C per 100 km and are associated with enhanced positive WSC exceeding 1.5×10^{-6} N/m³, and weakens progressively offshore. These regions coincide with cold upwelling zones associating with reduced wind stress magnitude (Figure 1b), and positive temperature gradients and WSC along the coast (Figure 1c). Both parameters decay offshore within approximately 150 km, matching the spatial extent of cold filaments and reduced wind stress (Figure 1c).

The analysis of the CWSG and WSC from 2003 to 2022 reveals strong coupling in the western Arabian Sea (Figure 1d). The Somalia upwelling region (4°N–10°N) exhibits the maximum coupling between WSC and CWSG, with a coupling coefficient of approximately 0.8, where positive WSC emerges with increasing CWSG. In contrast, the CWSG-WSC coupling coefficient in Oman upwelling region (17°N–20°N) is negative in coastal zones and gradually becomes positive offshore.

A pronounced coupling between WSC and CWSG is identified in the Somalia coastal upwelling region (6°N–11°N, 48°E–52°E), which serves as the core area for subsequent analysis due to its persistently strong air-sea interactions (Figures 1c, d). This region represents the most prominent upwelling system in the western Arabian Sea, where intense air-sea interactions provide an ideal setting for investigating WSC-CWSG coupling dynamics (McCreary et al., 1993; Schott et al., 2009). Dynamically, the area exhibits both high WSC intensity (WSC > 0.5×10^{-6} N/m³) and significant CWSG (CWSG > 0.7°C per 100km), with spatial correlation analysis revealing their strongest positive relationship (Figures 1c, d). The steep shelf topography enhances Ekman pumping processes, creating an orthogonal relationship between WSC and CWSG (Daae et al., 2017). This regional selection not only extends previous discussions of WSC-CWSG coupling mechanisms but also provides a basis for subsequent analyses grounded in clear dynamical explanations and sufficient observational evidence.

The spatial distribution of WSC and CWSG coupling in the western Arabian Sea exhibits distinct regional characteristics. In the Somalia upwelling region, strong spatial correlation is identified in the area with high CWSG and positive WSC (Figure 1), indicating significant positive coupling. This feature provides an ideal study area for investigating mesoscale air-sea interactions. Regions exhibiting strong WSC-CWSG coupling were identified and used to define the research domain through an integrated evaluation of multiple parameters (Figure 1d). The northern and southern boundaries are primarily determined by the positive CWSG range, with reference to the WSC positive distribution, while the eastern boundary is set at the transitional zone where the high CWSG nearshore decreases to near-zero values offshore. By excluding CWSG-negative regions north of 10°N and extending southward to 5°N to encompass the WSC maximum, the study area

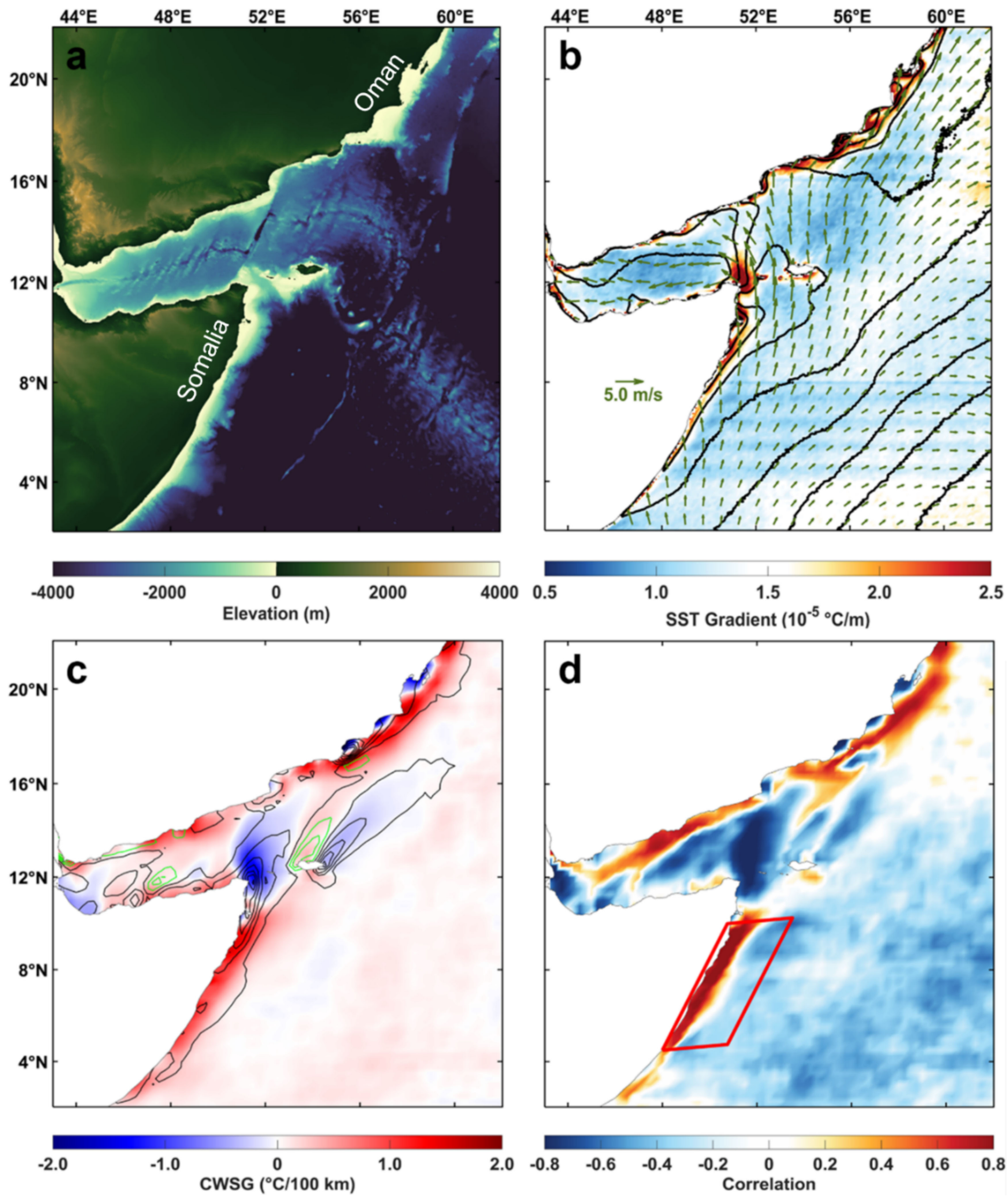

FIGURE 1
Spatial characteristics of topography, sea surface temperature (SST) gradients, and wind-ocean interaction in the western Arabian Sea. **(a)** Topographic map of the western Arabian Sea, with elevation and bathymetry (in meters) ranging from −4000 m (deep ocean basins) to 4000 m (high terrain). Color shading represents bathymetry, and major topographic features are labelled. **(b)** Annual average of SST gradient (°C per 100 km, color shading) with superimposed contours of SST (black lines; 0.5°C intervals) and vector-averaged wind speed (green arrows). **(c)** Crosswind SST gradient (units: °C per 100 km, shading) overlaid with wind stress curl (WSC) contours (green: negative; black: positive; interval: 2.0 N·m^{-2} per 10^4 km; zero contour omitted). **(d)** Temporal correlation map between crosswind SST gradient and WSC. The red box outlines the study region.

was defined to maximize scientific validity and regional representativeness (Figure 1c). It is noteworthy that although localized negative WSC-CWSG coupling coefficients exist, it effectively balances the trade-off between thermal feature resolution and spatial coverage while accounting for the inherent scale differences between large-scale WSC and mesoscale CWSG characteristics (O'Neill et al., 2003). More importantly, this framework highlights the Somalia upwelling as a key air-sea interaction zone, providing a reliable foundation for subsequent mesoscale process studies.

3.2 Spatiotemporal pattern of WSC-CWSG coupling in Somalia upwelling region

Following the previously established spatial delineation, the temporal period for this investigation is further defined. The May-September period is selected as the optimal temporal window for examining monsoon-forced upwelling dynamics along the coast of Somalia, as it fully encompasses the phenological cycle of Ekman upwelling (Figure 2). To ensure analytical robustness and climatological representativeness, the study period spans 2003-2022, which provides sufficient temporal coverage and access to high-resolution satellite observations. The rationale for this temporal selection is underpinned by several critical factors. First, the post-2003 era represents a paradigm shift in observational capabilities, with the operational deployment of advanced satellite constellations enabling continuous, high-resolution monitoring of essential ocean-atmosphere variables (Le Traon et al., 2015). This unprecedented increase in data availability significantly enhances spatial and temporal fidelity of analyses, thereby facilitating investigations of WSC-CWSG coupling mechanisms.

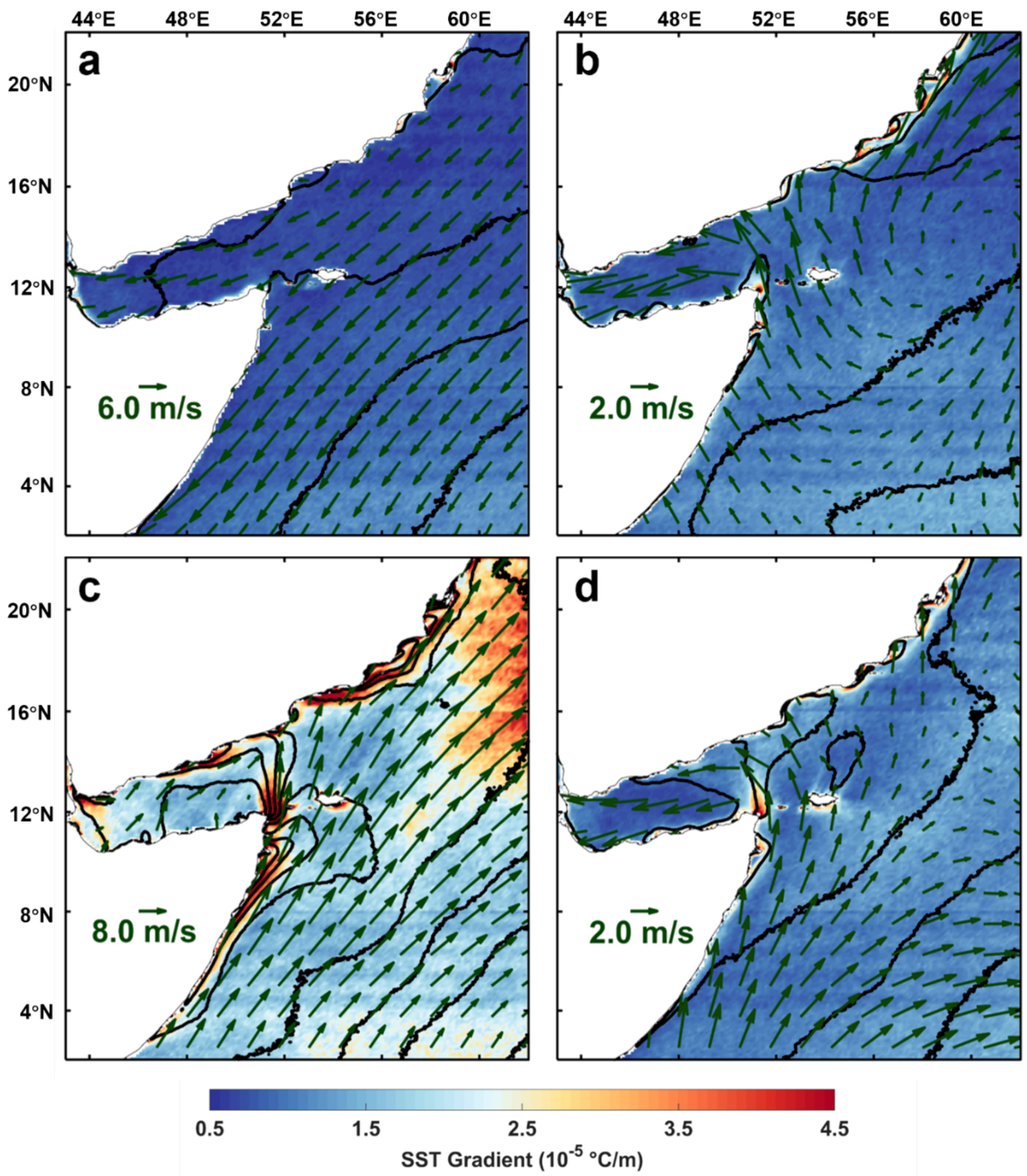

FIGURE 2
Seasonal variations of SST gradients and wind patterns. SST gradient (°C per 100 km, color shading) with superimposed contours of SST (black lines; 1.0°C intervals) and vector-averaged wind speed (black arrows) during **(a)** winter, **(b)** spring, **(c)** summer, **(d)** autumn.

Following the selection of temporal period, the temporal window was further refined through comprehensive analysis of seasonal hydrographic patterns. The western Arabian Sea exhibits marked seasonal contrasts in wind forcing and thermal responses (Figure 2). In spring, as the monsoon transitions, wind speeds decrease (~2 m/s), SST gradients begin to intensify (0.5–1.5°C per 100 km), and an cold tongue forms along the coast of Somalia (Figure 2a). Summer is characterized by strong southwest monsoon winds (8–16 m/s), driving a sharp increase in SST gradients (>4°C per 100 km) (Figure 2b). Intense upwelling along the Somalia-Oman coast brings cold subsurface water (as low as 22°C) to the surface, creating a strong thermal contrast with the surrounding warm oceanic waters (~30°C) (Wang et al., 2021). This cold tongue structure not only enhances air-sea temperature differences, providing positive feedback to the monsoon circulation (Vecchi et al., 2004), but also interacts with wind stress curl to modulate mesoscale eddies and boundary currents, demonstrating tight coupling between wind, thermal and dynamical processes (Wang and Castelao, 2016). By autumn, monsoon winds weaken (~2 m/s), upwelling subsides, and SST gradients decline to below 1°C per 100 km, leading to a more homogeneous surface thermal structure (Figure 2c). During winter, the northeast monsoon brings moderate winds (~6 m/s), while SST gradients remain weak (<0.5°C per 100 km), with relatively low and uniform SST (Figure 2d). Initial examination of the wind patterns, SST gradients, and upwelling intensities across all four seasons revealed that summer (June–August) exhibits the most pronounced conditions for studying WSC and CWSG interactions (Figures 1, 2). These summer conditions create ideal circumstances for investigating air-sea feedback mechanisms (McCreary et al., 1993).

The May–September period was chosen to capture the full evolution of monsoon-driven processes, as revealed by the seasonal patterns (Figure 3). During the incipient monsoon phase (May), moderate southeasterlies initiate primary upwelling near the equatorial zone. The transitional period (June) witnesses wind intensification and the emergence of a secondary cold wedge proximate to 8°–9°N, amplifying offshore Ekman transport. The mature monsoon phase (July–September) features persistent southwesterlies and the progressive northward advection of the upwelled cold-water mass (Schott and McCreary, 2001; Chatterjee et al., 2019). Though seasonal analysis determines summer is fully developed for coastal upwelling (Wang and LinHo, 2002), the delineation of summer-monsoon is more precisely conducted as the May–September, capturing both the peak intensity and complete developmental sequence of WSC-CWSG interactions (Xie and Philander, 1994). The extended timeframe facilitates examination of critical transitional periods that bookend the mature monsoon phase (Gadgil, 2003), thereby providing essential context for understanding the system's dynamical evolution while maintaining focus on the most scientifically relevant conditions for studying air-sea coupling mechanisms.

Validation of the temporal selection was achieved through comprehensive analysis of WSDS metrics and vector-averaged wind stress fields (Figure 3). This analysis reveals a distinct seasonal progression: the pre-monsoon period (April, Figure 3a) exhibits reduced WSDS magnitudes (0.7–0.8) under variable southeasterly flow; the core monsoon months (May–September, Figure 3b) demonstrate maximal WSDS values (~1.0), indicative of stable southwesterly forcing with peak wind stress intensity; and the post-monsoon transition (October, Figure 3c) shows declining WSDS (0.6–0.7) concomitant with wind vector rotation toward southerly orientations. This well-defined seasonal progression confirms that the May–September most effectively captures the fundamental WSC-CWSG coupling regime, while excluding

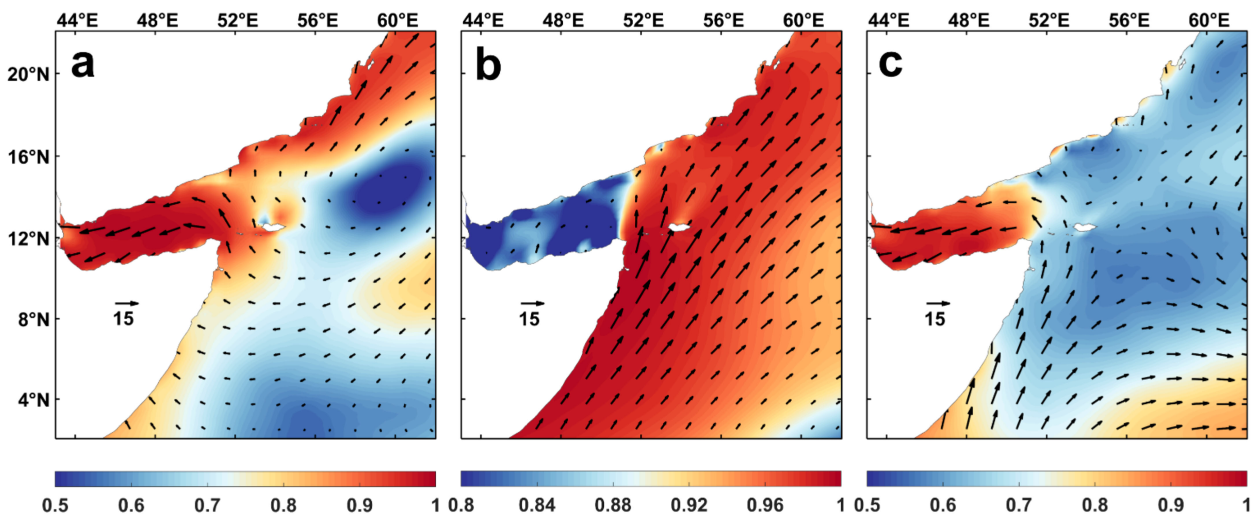

FIGURE 3
Map of wind stress directional steadiness (WSDS, color shading) overlaid with vector-averaged wind stress (10^{-2} N/m^2) for monsoon months **(a)** May, **(b)** summer (June–August), and **(c)** September.

transitional periods characterized by attenuated or less coherent forcing mechanisms (Tomczak and Godfrey, 1994). The synergistic combination of the defined temporal domain with the circumscribed study area supports an investigation of WSC-CWSG interactions that yields results accurately characterizing the upwelling dynamics.

3.3 Dynamical analysis of WSC-CWSG coupling

With the spatiotemporal framework established, the relationship between WSC and CWSG in the western Arabian Sea upwelling region is systematically examined, focusing on their regional and seasonal variability, with the time series of the two variables during monsoon months (Figure 4). In the Somalia upwelling region, the WSC and CWSG exhibit consistent temporal variations, indicating a strong coupling between atmospheric forcing and oceanic thermal gradients (Figures 4a, b). A remarkably strong linear correlation (R = 0.98) between WSC and CWSG anomalies is identified (Figure 4c), exceeding previously reported values for similar air-sea interactions (Chelton and Xie, 2010; O'Neill, 2012). This exceptionally high coupling coefficient provides compelling evidence for direct dynamical coupling between wind stress patterns and thermal fronts in this region. The relationship exhibits clear bidirectionality, suggesting the presence of mutual feedback mechanisms that maintain this tight coupling. The western Arabian Sea upwelling region exhibits pronounced WSC-CWSG coupling, facilitated by a unique combination of steep continental slope topography that enhances baroclinic response, sustained monsoonal wind forcing that maintains strong wind stress curl.

3.4 Importance of WSDS on regulating air-sea coupling

This study highlights the critical role of WSDS in modulating air-sea interactions, underpinned by a remarkably strong linear relationship between WSC and CWSG (r = 0.98) in the western Arabian Sea. The analysis reveals distinct temporal variations in coupling coefficients, closely linked to the stability of monsoon-driven winds. During the established monsoon period (May–September), WSDS maintains consistently high values (~1.0), coinciding with robust WSC-CWSG coupling. In contrast, transitional seasons (particularly April and October) exhibit pronounced declines in WSDS (0.6–0.7) where the coupling coefficient weakens significantly or even reverses (Figure 5b). The WSDS modulates air-sea coupling through complementary temporal and spatial mechanisms. Temporally, sustained WSDS conditions (>0.85 for periods exceeding seven days) enhance wind forcing persistence. Spatially, stable wind directions (WSDS>0.88 during peak monsoon months) promote more organized thermal structures by reducing CWSG variability by approximately 0.2°C per 100km for every 0.1 WSDS increase. These findings reveal WSDS as both an indicator and active modulator of coupling strength, with particular significance during monsoon transitions (Renault et al., 2019). The onset period's unstable winds (WSDS<0.7) disrupt coupling development, as demonstrated by Vialard et al. (2012) who observed a 55% reduction in Ekman pumping efficiency during such periods, while subsequent stabilization enables full expression of ocean-atmosphere interactions.

The standardized offshore profiles of monthly WSC-CWSG and corresponding coupling coefficients was investigated from May to October (Figure 6). The monthly coefficients demonstrate consistently strong coupling throughout the summer: 0.80 (May), 0.86 (June), 0.86 (July), 0.88 (August), and 0.93 (September), exhibiting a clear monotonic increase, peaking in September. This

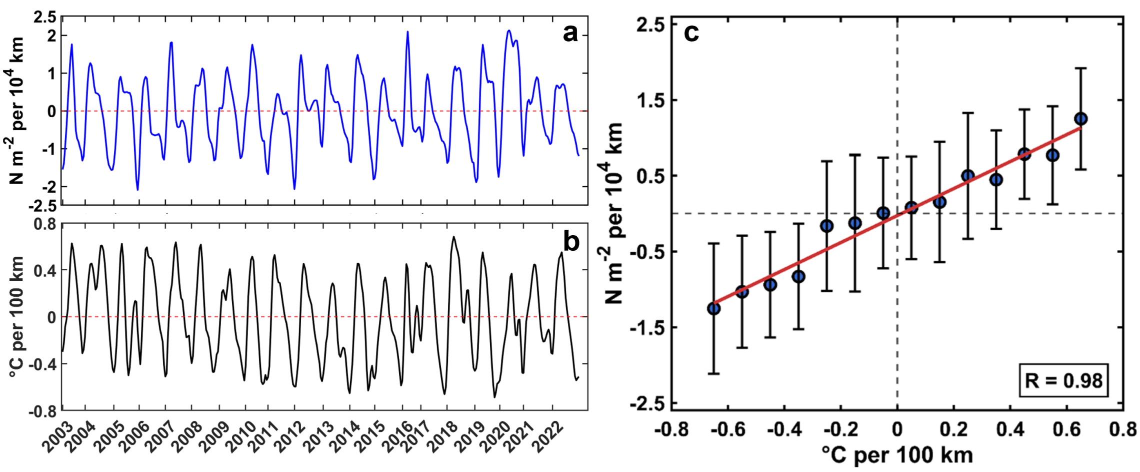

FIGURE 4
Relationship between WSC and crosswind SST gradient. **(a)** Time series of WSC during the monsoon period (May–September), with units of 10^{-7} N/m^3. **(b)** Time series of crosswind SST gradient, with units of °C per 100 km. The x-axis in both **(a, b)** represents 7-day averaged data points over 20 years (2003–2022), covering all available summer observations. **(c)** Bin-averaged relationship between WSC and CWSG in the western Arabian Sea (see box in Figure 1d), based on anomaly fields. Vertical error bars indicate the standard deviation within each bin, and the coupling coefficients (R) is noted in the panel.

progression reveals significant seasonal modulation between WSC-CWSG, with the strongest coupling coefficients occurring during late summer monsoon. The abrupt reversal to negative coupling coefficient (R = -0.17) in October coincides with the monsoon transition period, as changing wind patterns and reduced WSC disrupt the established summer coupling dynamics (Schott et al., 2009). The annual coupling coefficient range of 0.8–0.9 during summer months confirms a robust positive relationship when WSC most directly governs thermal gradient distribution, while the October anomaly underscores the quick responds due to seasonal forcing changes. The spatial patterns clearly demonstrate that WSC exerts its strongest influence on SST gradients in the upwelling-dominated coastal region, with the effects diminishing substantially offshore (Figure 6). Within 50 km of the coastline, this coupling is particularly intense, driven by a combination of synergistic mechanisms. Steep coastal topography amplifies Ekman pumping, intensifying vertical transport of subsurface waters (Shankar et al., 2002).

The monotonic increase in coupling coefficients from May (0.80) to September (0.93) demonstrates the critical role of WSDS in mediating the WSC-CWSG relationship. With WSDS maintaining near-unity values (~1.0) throughout this period, the progressively stronger coupling reflects the cumulative effect of stable wind forcing enabling full development of mesoscale air-sea interactions (Figure 5). The month-by-month enhancement suggests that prolonged exposure to high WSDS conditions (>0.85) systematically strengthens the interaction between SST gradient and WSC, as evidenced by the prominent increase in coupling coefficients over the monsoon period (Figure 6). This temporal progression highlights how wind direction stability acts as both a prerequisite and amplifier for effective coupling, where persistently high WSDS provides the necessary conditions for interaction.

4 Discussion

The ocean-atmosphere interaction over the summer upwelling region in the western Arabian Sea examines with MODIS SST and ERA5 wind stress datasets. The topographic configuration of the region exerts a fundamental influence on coastal upwelling intensity during the southwest monsoon. Regions with narrow continental shelves and steep slopes, particularly along the Somalia coast where depths exceed 2,000 m within close proximity to the shoreline, promote highly efficient vertical transport of cold, nutrient-rich deep water. This topographically enhanced upwelling, driven by persistent alongshore monsoonal winds and associated Ekman transport, sustains elevated nutrient availability and primary

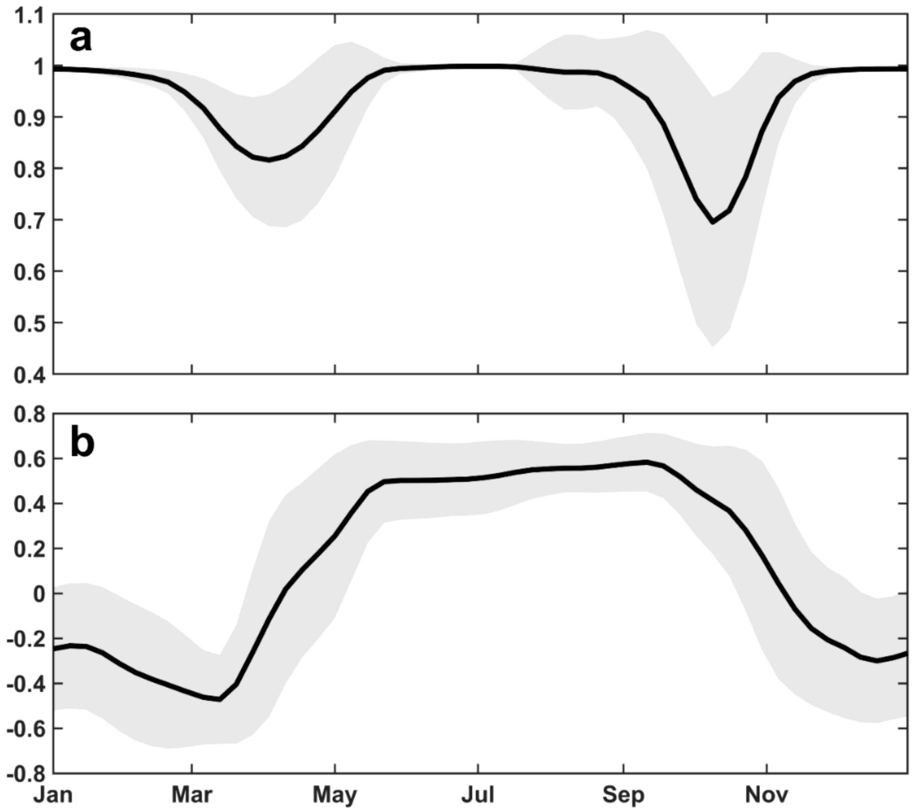

FIGURE 5
Time series of **(a)** averaged WSDS and **(b)** the coupling coefficients between WSC and the crosswind SST gradient in the western Arabian Sea (see the box in Figure 1d). The shading in both panels represents the standard deviation calculated from multi-year data for the corresponding time of year.

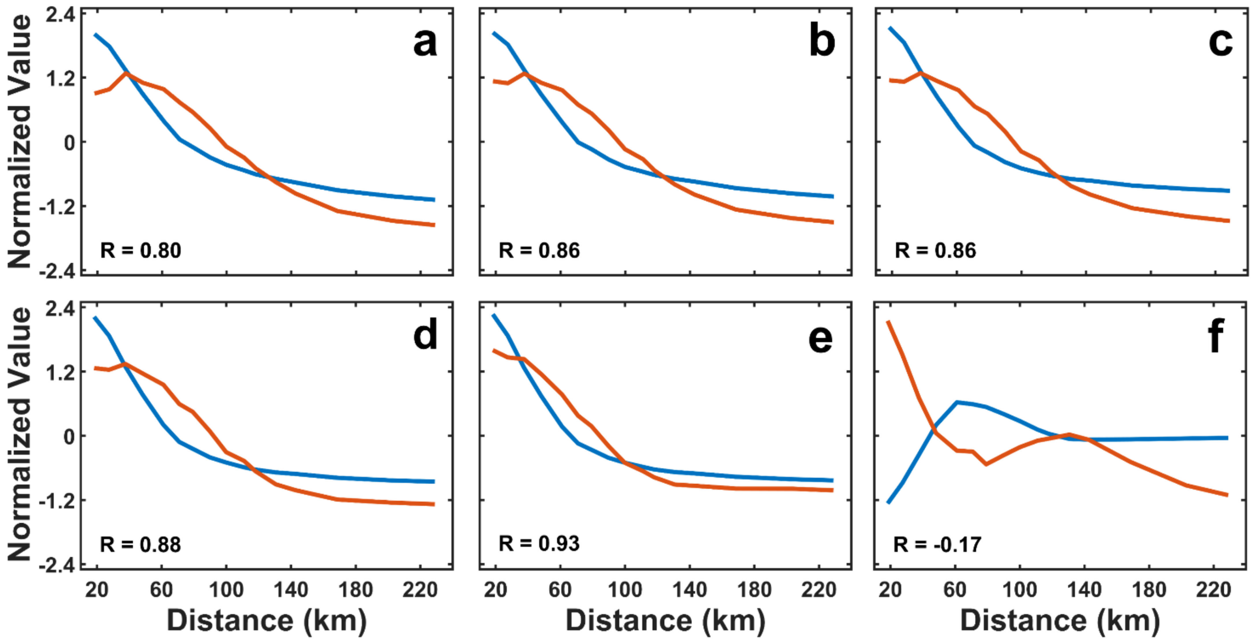

FIGURE 6
Normalized profiles of WSC (blue curves) and CWSG (orange curves) versus offshore distance (10–240 km). The vertical axis represents normalized values, while the horizontal axis denotes distance in kilometers. Panels **(a–f)** correspond to May, June, July, August, September and October, respectively.

productivity, in line with other upwelling-dominated systems (Beal et al., 2000; Lakshmi et al., 2020).

These physical processes are clearly expressed in the spatial distribution of SST anomalies. Notably, the Somalia upwelling front exhibits an exceptionally steep SST gradient (>7 °C per 100 km), indicative of an intense oceanic frontal system that enhances vertical nutrient flux and supports vigorous biological production (Schott et al., 2009; Lakshmi et al., 2020). In contrast, moderate SST gradients were observed off Oman (2–3 °C per 100 km), likely reflecting topographically mediated weakening of monsoon winds (Yi et al., 2018). In the central western Arabian Sea, SST gradients are minimal (<1 °C per 100 km), consistent with regions of wind stress convergence and weak surface forcing that limit vertical mixing and suppress thermal structure. Together, these regional patterns highlight the strong modulation of upwelling by both wind forcing and coastal bathymetry. Moreover, dynamic feedback exists as wind-driven SST gradients reshape ABL stability and in turn alter surface wind fields, reinforcing the complexity of air-sea coupling in the monsoon-dominated western Arabian Sea (Schott et al., 2009; Small et al., 2008).

The regional coupling patterns between WSC and CWSG further elucidate the spatial structure of monsoon-driven upwelling coupling in the western Arabian Sea, particularly across the Somalia and Oman upwelling regions (Figure 1d). In the Somalia upwelling region, this relationship is particularly pronounced ($r \approx 0.8$), indicating that WSC responds sensitively to underlying SST fronts. This observation is in consistent with established feedback mechanisms, whereby sharp SST gradients modulate the overlying ABL, altering wind stress patterns and reinforcing ocean-atmosphere interactions (Chelton et al., 2004). However, this coupling weakens markedly in the northwestern Arabian Sea, particularly between 17°N and 20°N, where coupling coefficients decline significantly. This spatial disparity reflects the disruptive influence of coastal topography that prominent capes and coastal curvature can distort local wind stress patterns (Chelton et al., 2007), and numerical studies confirm the coastal terrain can attenuate wind stress magnitudes by 10–80% within 10–80 km offshore (Renault et al., 2016).

The exceptionally large coupling coefficients between WSC and CWSG observed in this study ($R = 0.98$) surpasses values previously reported for similar air-sea interaction systems (Chelton and Xie, 2010; O'Neill, 2012), offering compelling evidence for direct dynamical coupling between wind stress patterns and oceanic thermal fronts. This finding supports theoretical expectations from ABL models (Small et al., 2008) and further confirms the presence of mutual feedback mechanisms proposed in high-resolution coupled simulations (Renault et al., 2019). The bidirectional nature of this coupling suggests that WSC may not only drive but also be modulated by SST gradients, reinforcing the view of a tightly integrated air-sea feedback system. It also reflects a combination of unique geophysical and climatic factors. Specifically, the region's steep continental slope enhances Ekman pumping efficiency by facilitating rapid vertical transport of subsurface waters (Schott and McCreary, 2001), while the strong and persistent southwest monsoon winds maintain background gradients conducive to intensified air-sea interaction (Currie et al., 2013). Moreover, minimal summer cloud cover (typically<20%) allows for high-precision satellite retrievals of both wind vectors and SST fields, which reduces observational uncertainty (Vialard et al., 2009). These regional characteristics collectively contribute to the pronounced WSC-CWSG coupling signal observed here, underscoring how topography and wind regimes jointly modulate air-sea dynamics, which can be dedicatedly depicted with high atmospheric clarity. Such a robust relationship implies close dependence between WSC and CWSG, with the potential to improve short-term oceanographic forecasts by 15–20%, consistent with predictive gains reported in other upwelling systems (Chelton and Xie, 2010; Renault et al., 2019).

The WSDS is confirmed to serve as a pivotal regulator of mesoscale air-sea interactions in the western Arabian Sea, exhibiting pronounced seasonal modulation under the influence of the South Asian monsoon system. During the boreal summer, persistently strong and highly unidirectional southwesterly winds foster exceptionally high WSDS values (>0.95), thereby creating an optimal dynamical regime for robust coupling between WSC and CWSG (Figure 3b). During periods of elevated WSDS (Figure 5), WSC and CWSG exhibit stronger coupling coefficients with an approximately linear relationship (Figure 4c), indicating a stable and direct dynamical linkage between them. The coupling coefficients between these two fields further exhibit a monotonic strengthening from May to September, reflecting the progressive intensification of monsoonal forcing and air-sea interaction (Figure 6). The persistence of stable monsoonal winds enhances Ekman pumping efficiency by prolonging atmospheric forcing, thereby reinforcing oceanic responses over time (Chelton et al., 2007). Observations indicate that coupling strength can increase by 30–40% during periods of high wind stability, such as the mature monsoon phase (Chatterjee et al., 2019).

By contrast, during the winter monsoon, the intrusion of weaker, variable northeasterly winds originating from the continental interior results in substantially lower WSDS (<0.6), leading to a marked collapse in the strength of WSC-CWSG coupling (Vialard et al., 2012). The suppression of upwelling, diminished SST gradients, and disorganized ABL structures collectively inhibit the maintenance of air-sea feedbacks, consistent with earlier observational syntheses (Shankar et al., 2002; Schott et al., 2009). Transitional seasons reveal an intermediate regime: during spring, the progressive buildup of WSDS initiates the strengthening of coupling; whereas in autumn, the decay of WSDS post-monsoon onset precipitates rapid de-coupling, even when residual SST anomalies persist (Figure 5). Spatially, stable wind directions promote the development of coherent thermal structures and facilitate more efficient momentum and energy transfer across the air-sea interface (Small et al., 2008; Belcher et al., 2012). In particular, the sharp decline and reversal of the WSC-CWSG correlation in October can be attributed to the seasonal transition of monsoonal wind forcing (Figure 6f). As the southwest monsoon weakens and transitions into the northeast monsoon, the prevailing wind direction shifts, reducing the alongshore wind stress that previously sustained upwelling (Schott et al., 2009). This transition disrupts the Ekman-driven offshore transport and weakens the coastal frontal gradients, thereby diminishing the coupling strength between WSC and CWSG (Xie, 2004). Additionally, the ocean adjusts to this forcing change through baroclinic processes such as coastally trapped waves and subsurface thermal structure adjustments, which further decouple the surface wind from the coastal upwelling signal (McCreary et al., 1993). These combined effects likely explain the breakdown in WSC-CWSG coherence observed in October.

In addition to the seasonal modulation, a striking spatial heterogeneity emerges, featuring a pronounced coastal intensification of WSC-CWSG coupling strength (Figure 1c). During the summer monsoon, large coupling coefficients exceeding 0.9 occurred within 100 km off the coast of Somalia, then decay rapidly offshore in an approximately exponential fashion (Figure 1d), aligning with previous observations of localized upwelling dynamics (Vialard et al., 2012). Several interacting coastal processes are simultaneously driving the dynamics. First, the steep coastal bathymetry significantly enhances Ekman pumping, under persistent cross-shore monsoonal winds, promoting strong upwelling (Figure 1a). Second, the shallow mixed layers (~20–30 m) observed during the early monsoon season increase SST sensitivity to atmospheric forcing, thereby accelerating the air-sea feedback loop (Small et al., 2008). Third, nearshore regions experience reduced lateral advection, allowing sharp thermal gradients to persist and reinforcing the coherence of mesoscale SST structures (Chelton et al., 2007). These gradients, in turn, help sustain atmospheric responses via ABL instabilities (Gaube et al., 2015). Together, these mechanisms explain the coastal intensification of coupling and underscore the critical role of regional bathymetry and hydrography in modulating air-sea interactions.

The western Arabian Sea presents fundamentally similar patterns to other major upwelling-dominated boundary currents, such as the California and Benguela systems (Renault et al., 2019), where strong nearshore coupling occurs in regions with sharp SST gradients and narrow coastal jets (Figure 1). However, it departs markedly in its temporal dynamics, displaying a binary seasonal transition between robustly coupled summer states and largely decoupled winter conditions. This behavior is fundamentally rooted in the unique monsoon-driven wind regime, which imposes sharp seasonality absent in trade-wind dominated systems (Figure 2).

A particularly novel aspect of the western Arabian Sea is the regional decoupling of downwind SST gradient (DWSG) and wind stress divergence (WSD) along the coast of Somalia, even in the presence of strong upwelling and sharp thermal fronts. Whereas classical ABL instability theory would predict strong DWSG-WSD coupling under such conditions (Chelton et al., 2010), we observe weak coupling coefficients (R<0.3), attributable to an approximate 90° misalignment between southwesterly monsoon winds and the orientation of SST fronts (Figure 1b). This geometric constraint effectively minimizes DWSG, undermining typical baroclinic adjustment mechanisms (Chelton et al., 2007; Tamsitt et al., 2016). Additionally, the strong remote forcing exerted by the

Findlater Jet (Xie and Philander, 1994) likely overwhelms local SST-induced perturbations, further weakening DWSG-WSD coupling. This regional decoupling highlights the need for location-specific frameworks when diagnosing mesoscale air-sea interactions, challenging the universality of coupling paradigms developed in eastern boundary systems.

The demonstrated modulation of coupling strength by WSDS has significant implications for climate modeling and prediction. Most current coupled models lack an explicit treatment of WSDS variability, potentially limiting their ability to faithfully simulate seasonal SST structure and monsoon dynamics. Our findings highlight the need to incorporate WSDS based parameterizations into coupled models, particularly in monsoon influence. Specifically, quantifying the degree of air-sea coupling to explain wind direction persistence, coupled with high-resolution ocean-atmosphere grids, will be a crucial step forward (Small et al., 2008). From the perspective of physical mechanisms, variations in WSDS covary with other wind stress variables such as wind speed and WSC, making it difficult for existing signal separation and causal identification methods to effectively distinguish the independent contributions of each factor to vertical momentum mixing (Renault et al., 2016). Future work should develop advanced methods to separate the WSDS effect from other wind stress variables to better constrain the temporal evolution of mesoscale feedback mechanisms.

In summary, the study advances the understanding of mesoscale air-sea interactions by quantifying WSDS as a dynamic regulator of coupling strength, elucidating the geometric constraints underlying regional decoupling, and articulating the implications for next-generation climate modeling frameworks. These insights contribute to a growing recognition of the complexity and regional specificity of ocean-atmosphere feedbacks in the global climate system.

5 Conclusion

This study highlights the significant role of WSDS in modulating ocean-atmosphere interactions in the western Arabian Sea, particularly during the monsoon seasons. Understanding these dynamics not only enhances our knowledge of regional climate processes but also contributes to broader climate models that incorporate ocean-atmosphere coupling mechanisms. WSDS is a pivotal yet overlooked factor in western Arabian Sea air-sea interactions. High wind steadiness during summer facilitates strong mesoscale coupling via upwelling fronts, while transitional seasons exhibit phase-dependent coupling tied to monsoon dynamics. Future work should explore biogeochemical responses and extend this framework to other monsoon basins.

Data availability statement

The original contributions presented in the study are included in the article/supplementary material. Further inquiries can be directed to the corresponding author/s.

Author contributions

XL: Visualization, Formal analysis, Writing – original draft, Investigation. SB: Writing – review & editing, Methodology, Validation. YW: Supervision, Conceptualization, Writing – review & editing.

Funding

The author(s) declare that financial support was received for the research and/or publication of this article. This study is funded by National Natural Science Foundation of China (No. 42176013) and the Zhejiang Provincial Natural Science Foundation of China (No. LR25D060001). The study is conducted as a joint effort through the UN Decade of Ocean Science for Sustainable Development (2021-2030) endorsed action Mitigation of Natural Incidence Towards an increased Oceanic Resilience (MoNITOR).

Conflict of interest

The authors declare that the research was conducted in the absence of any commercial or financial relationships that could be construed as a potential conflict of interest.

Generative AI statement

The author(s) declare that no Generative AI was used in the creation of this manuscript.

Publisher's note

References

Barnes, W. L., and Salomonson, V. V. (1995). "Design and projected performance of MODIS — A moderate-resolution imaging spectroradiometer for the earth observing system (EOS)," in *Applications of Photonic Technology*. Eds. G. A. Lampropoulos, J. Chrostowski and R. M. Measures (Springer US, Boston, MA), 171–178. doi: 10.1007/978-1-4757-9247-8_34

Beal, L. M., and Donohue, K. A. (2013). The great whirl: observations of its seasonal development and interannual variability. *J. Geophysical Res.* 118, 1–13. doi: 10.1029/2012JC008198

Beal, L. M., Molinari, R. L., Chereskin, T. K., and Robbins, P. E. (2000). Reversing bottom circulation in the somali basin. *Geophysical Res. Lett.* 27, 2565–2568. doi: 10.1029/1999GL011316

Belcher, S. E., Grant, A. L. M., Hanley, K. E., Fox-Kemper, B., Van Roekel, L., Sullivan, P. P., et al. (2012). A global perspective on langmuir turbulence in the ocean surface boundary layer. *Geophysical Res. Lett.* 39, 2012GL052932. doi: 10.1029/2012GL052932

Bourassa, M. A., Gille, S. T., Bitz, C., Carlson, D., Cerovecki, I., Clayson, C. A., et al. (2013). High-latitude ocean and sea ice surface fluxes: challenges for climate research. *Bull. Am. Meteorological Soc.* 94, 403–423. doi: 10.1175/BAMS-D-11-00244.1

Bryan, F. O., Tomas, R., Dennis, J. M., Chelton, D. B., Loeb, N. G., and McClean, J. L. (2010). Frontal scale air–sea interaction in high-resolution coupled climate models. *J. Climate* 23, 6277–6291. doi: 10.1175/2010JCLI3665.1

Castelao, R. M. (2012). Sea surface temperature and wind stress curl variability near a cape. *J. Phys. Oceanography* 42, 2073–2087. doi: 10.1175/JPO-D-11-0224.1

Chatterjee, A., Kumar, B. P., Prakash, S., and Singh, P. (2019). Author correction: annihilation of the somali upwelling system during summer monsoon. *Sci. Rep.* 9, 18903. doi: 10.1038/s41598-019-54632-x

Chelton, D. B., Esbensen, S. K., Schlax, M. G., Thum, N., Freilich, M. H., Wentz, F. J., et al. (2001). Observations of coupling between surface wind stress and sea surface temperature in the eastern tropical pacific. *J. Climate* 14, 20. doi: 10.1175/1520-0442(2001)014<1479:OOCBSW>2.0.CO;2

Chelton, D. B., Schlax, M. G., Freilich, M. H., and Milliff, R. F. (2004). Satellite measurements reveal persistent small-scale features in ocean winds. *Science* 303, 978–983. doi: 10.1126/science.1091901

Chelton, D. B., Schlax, M. G., and Samelson, R. M. (2007). Summertime coupling between sea surface temperature and wind stress in the california current system. *J. Phys. Oceanography* 37, 495–517. doi: 10.1175/JPO3025.1

Chelton, D., and Xie, S.-P. (2010). Coupled ocean-atmosphere interaction at oceanic mesoscales. *Oceanography* 23, 52–69. doi: 10.5670/oceanog.2010.05

Chen, X., Dewar, W., Chassignet, E., Bourassa, M., Morey, S., and Gopalakrishnan, G. (2022). On the feedback between air-sea turbulent momentum flux and oceanic submesoscale processes. *J. Geophysical Research: Oceans* 127, e2022JC018767. doi: 10.1029/2022JC018767

Cronin, M. F., Gentemann, C. L., Edson, J., Ueki, I., Bourassa, M., Brown, S., et al. (2019). Air-sea fluxes with a focus on heat and momentum. *Front. Mar. Sci.* 6. doi: 10.3389/fmars.2019.00430

Cui, C., Zhang, R.-H., Wang, H., and Wei, Y. (2020). Representing surface wind stress response to mesoscale SST perturbations in western coast of South America using tikhonov regularization method. *J. Oceanology Limnology* 38, 679–694. doi: 10.1007/s00343-019-9042-8

Currie, J. C., Lengaigne, M., Vialard, J., Kaplan, D. M., Aumont, O., Naqvi, S. W. A., et al. (2013). Indian ocean dipole and el niño/southern oscillation impacts on regional chlorophyll anomalies in the Indian ocean. *Biogeosciences* 10, 6677–6698. doi: 10.5194/bg-10-6677-2013

Czaja, A., and Frankignoul, C. (2002). Observed impact of atlantic SST anomalies on the North Atlantic Oscillation. *J. Climate* 15, 606–623. doi: 10.1175/1520-0442(2002)015<0606:OIOASA>2.0.CO;2

Daae, K., Hattermann, T., Darelius, E., and Fer, I. (2017). On the effect of topography and wind on warm water inflow-an idealized study of the Southern Weddell sea continental shelf system. *J. Geophysical Research: Oceans* 122, 2622–2641. doi: 10.1002/2016JC012541

Deser, C., Alexander, M. A., Xie, S.-P., and Phillips, A. S. (2010). Sea surface temperature variability: patterns and mechanisms. *Annu. Rev. Mar. Sci.* 2, 115–143. doi: 10.1146/annurev-marine-120408-151453

Frankignoul, C., and Hasselmann, K. (1977). Stochastic climate models, part II application to sea-surface temperature anomalies and thermocline variability. *Tellus A: Dynamic Meteorology Oceanography* 29, 289. doi: 10.3402/tellusa.v29i4.11362

Frenger, I., Gruber, N., Knutti, R., and Münnich, M. (2013). Imprint of southern ocean eddies on winds, clouds and rainfall. *Nat. Geosci.* 6, 608–612. doi: 10.1038/ngeo1863

Frenger, I., Münnich, M., Gruber, N., and Knutti, R. (2015). Southern ocean eddy phenomenology. *J. Geophysical Research: Oceans* 120, 7413–7449. doi: 10.1002/2015JC011047

Gadgil, S. (2003). The Indian monsoon and its variability. *Annu. Rev. Earth Planetary Sci.* 31, 429–467. doi: 10.1146/annurev.earth.31.100901.141251

Gaube, P., Chelton, D. B., Samelson, R. M., Schlax, M. G., and O'Neill, L. W. (2015). Satellite observations of mesoscale eddy-induced ekman pumping. *J. Phys. Oceanography* 45, 104–132. doi: 10.1175/JPO-D-14-0032.1

Hayes, S. P., McPhaden, M. J., and Wallace, J. M. (1989). The influence of sea-surface temperature on surface wind in the eastern equatorial pacific: weekly to monthly variability. *J. Climate* 2, 1500–1506. doi: 10.1175/1520-0442(1989)002<1500:TIOSST>2.0.CO;2

Hersbach, H., Bell, B., Berrisford, P., Hirahara, S., Horányi, A., Muñoz-Sabater, J., et al. (2020). The ERA5 global reanalysis. *Q. J. R. Meteorological Soc.* 146, 1999–2049. doi: 10.1002/qj.3803

Kilpatrick, K. A., Podestá, G., Walsh, S., Williams, E., Halliwell, V., Szczodrak, M., et al. (2015). A decade of sea surface temperature from MODIS. *Remote Sens. Environ.* 165, 27–41. doi: 10.1016/j.rse.2015.04.023

Lakshmi, R. S., Chatterjee, A., Prakash, S., and Mathew, T. (2020). Biophysical interactions in driving the summer monsoon chlorophyll bloom off the Somalia coast. *J. Geophysical Res.* 125, e2019JC015549. doi: 10.1029/2019JC015549

Le Traon, P.-Y., Antoine, D., Bentamy, A., Bonekamp, H., Breivik, L. A., Chapron, B., et al. (2015). Use of satellite observations for operational oceanography: recent achievements and future prospects. *J. Operational Oceanography* 8, s12–s27. doi: 10.1080/1755876X.2015.1022050

Ma, X., Chang, P., Saravanan, R., Montuoro, R., Nakamura, H., Wu, D., et al. (2017). Importance of resolving kuroshio front and eddy influence in simulating the North Pacific storm track. *J. Climate* 30, 1861–1880. doi: 10.1175/JCLI-D-16-0154.1

Ma, X., Jing, Z., Chang, P., Liu, X., Montuoro, R., Small, R. J., et al. (2016). Western boundary currents regulated by interaction between ocean eddies and the atmosphere. *Nature* 535, 533–537. doi: 10.1038/nature18640

McCreary, J. P., Kundu, P. K., and Molinari, R. L. (1993). A numerical investigation of dynamics, thermodynamics and mixed-layer processes in the Indian ocean. *Prog. Oceanography* 31, 181–244. doi: 10.1016/0079-6611(93)90002-U

O'Neill, L. W. (2012). Wind speed and stability effects on coupling between surface wind stress and SST observed from buoys and satellite. *J. Climate* 25, 1544–1569. doi: 10.1175/JCLI-D-11-00121.1

O'Neill, L. W., Chelton, D. B., and Esbensen, S. K. (2003). Observations of SST-induced perturbations of the wind stress field over the Southern Ocean on seasonal timescales. *J. Climate* 16, 2340–2354. doi: 10.1175/2780.1

O'Neill, L. W., Chelton, D. B., and Esbensen, S. K. (2010). The effects of SST-induced surface wind speed and direction gradients on midlatitude surface vorticity and divergence. *J. Climate* 23, 255–281. doi: 10.1175/2009JCLI2613.1

O'Reilly, C. H., and Czaja, A. (2015). The response of the pacific storm track and atmospheric circulation to kuroshio extension variability. *Q. J. R. Meteorological Soc.* 141, 52–66. doi: 10.1002/qj.2334

Oerder, V., Colas, F., Echevin, V., Masson, S., Hourdin, C., Jullien, S., et al. (2016). Mesoscale SST–wind stress coupling in the Peru–Chile current system: which mechanisms drive its seasonal variability? *Climate Dynamics* 47, 2309–2330. doi: 10.1007/s00382-015-2965-7

Park, K., and Cornillon, P. C. (2002). Stability-induced modification of sea surface winds over gulf stream rings. *Geophysical Res. Lett.* 29(24), 2211. doi: 10.1029/2001GL014236

Renault, L., Masson, S., Oerder, V., Jullien, S., and Colas, F. (2019). Disentangling the mesoscale ocean-atmosphere interactions. *J. Geophysical Research: Oceans* 124, 2164–2178. doi: 10.1029/2018JC014628

Renault, L., Molemaker, M. J., McWilliams, J. C., Shchepetkin, A. F., Lemarié, F., Chelton, D., et al. (2016). Modulation of wind work by oceanic current interaction with the atmosphere. *J. Phys. Oceanography* 46, 1685–1704. doi: 10.1175/JPO-D-15-0232.1

Schott, F. A., and McCreary, J. P. (2001). The monsoon circulation of the Indian ocean. *Prog. Oceanography* 51, 1–123. doi: 10.1016/S0079-6611(01)00083-0

Schott, F. A., Xie, S., and McCreary, J. P. (2009). Indian ocean circulation and climate variability. *Rev. Geophysics* 47, 2007RG000245. doi: 10.1029/2007RG000245

Shankar, D., Vinayachandran, P. N., and Unnikrishnan, A. S. (2002). The monsoon currents in the North Indian ocean. *Prog. Oceanography* 52, 63–120. doi: 10.1016/S0079-6611(02)00024-1

Shao, M., Ortiz-Suslow, D. G., Haus, B. K., Lund, B., Williams, N. J., Özgökmen, T. M., et al. (2019). The variability of winds and fluxes observed near submesoscale fronts. *J. Geophysical Research: Oceans* 124, 7756–7780. doi: 10.1029/2019JC015236

Small, R. J., deSzoeke, S. P., Xie, S. P., O'Neill, L., Seo, H., Song, Q., et al. (2008). Air–sea interaction over ocean fronts and eddies. *Dynamics Atmospheres Oceans* 45, 274–319. doi: 10.1016/j.dynatmoce.2008.01.001

Small, R. J., Xie, S.-P., and Wang, Y. (2003). Numerical simulation of atmospheric response to pacific tropical instability waves. *J. Climate* 16, 3723–3741. doi: 10.1175/1520-0442(2003)016<3723:NSOART>2.0.CO;2

Sullivan, P. P., and McWilliams, J. C. (2010). Dynamics of winds and currents coupled to surface waves. *Annu. Rev. Fluid Mechanics* 42, 19–42. doi: 10.1146/annurev-fluid-121108-145541

Sun, S., Fang, Y., Zu, Y., Liu, B., Tana,, and Samah, A. A. (2020). Seasonal characteristics of mesoscale coupling between the sea surface temperature and wind speed in the South China sea. *J. Climate* 33, 625–638. doi: 10.1175/JCLI-D-19-0392.1

Tamsitt, V., Talley, L. D., Mazloff, M. R., and Cerovečki, I. (2016). Zonal variations in the southern ocean heat budget. *J. Climate* 29, 6563–6579. doi: 10.1175/JCLI-D-15-0630.1

Tomczak, M., and Godfrey, J. S. (1994). "Antarctic oceanography," in *Regional Oceanography* (Melbourne, Australia: Elsevier), 67–87. doi: 10.1016/B978-0-08-041021-0.50010-2

Vecchi, G. A., Xie, S.-P., and Fischer, A. S. (2004). Ocean–atmosphere covariability in the western Arabian sea. *J. Climate* 17, 1213–1224. doi: 10.1175/1520-0442(2004)017<1213:OCITWA>2.0.CO;2

Vialard, J., Jayakumar, A., Gnanaseelan, C., Lengaigne, M., Sengupta, D., and Goswami, B. N. (2012). Processes of 30–90 days sea surface temperature variability in the Northern Indian ocean during boreal summer. *Climate Dynamics* 38, 1901–1916. doi: 10.1007/s00382-011-1015-3

Vialard, J., Shenoi, S. S. C., McCreary, J. P., Shankar, D., Durand, F., Fernando, V., et al. (2009). Intraseasonal response of the Northern Indian ocean coastal waveguide to the madden-julian oscillation. *Geophysical Res. Lett.* 36, 2009GL038450. doi: 10.1029/2009GL038450

Wallace, J. M., Mitchell, T. P., and Deser, C. (1989). The influence of sea-surface temperature on surface wind in the eastern equatorial pacific: seasonal and interannual variability. *J. Climate* 2, 1492–1499. doi: 10.1175/1520-0442(1989)002<1492:TIOSST>2.0.CO;2

Wang, Y., and Castelao, R. M. (2016). Variability in the coupling between sea surface temperature and wind stress in the global coastal ocean. *Continental Shelf Res.* 125, 88–96. doi: 10.1016/j.csr.2016.07.011

Wang, Y., Ma, W., Zhou, F., and Chai, F. (2021). Frontal variability and its impact on chlorophyll in the arabian sea. *J. Mar. Syst.* 218, 103545. doi: 10.1016/j.jmarsys.2021.103545

Wenegrat, J. O., and Arthur, R. S. (2018). Response of the atmospheric boundary layer to submesoscale sea surface temperature fronts. *Geophysical Res. Lett.* 45(13), 505–13,512. doi: 10.1029/2018GL081034

Wikle, C. K. (2015). Modern perspectives on statistics for spatio-temporal data. *Wiley Interdiscip. Rev.* 7, 86–98. doi: 10.1002/wics.1341

Xie, S.-P. (2004). Satellite observations of cool ocean–atmosphere interaction. *Bull. Am. Meteorological Soc.* 85, 195–208. doi: 10.1175/BAMS-85-2-195

Xie, S.-P., and Philander, S. G. H. (1994). A coupled ocean-atmosphere model of relevance to the ITCZ in the Eastern Pacific. *Tellus A: Dynamic Meteorology Oceanography* 46, 340. doi: 10.3402/tellusa.v46i4.15484

Yi, X., Hünicke, B., Tim, N., and Zorita, E. (2018). The relationship between arabian sea upwelling and Indian monsoon revisited in a high resolution ocean simulation. *Climate Dynamics* 50, 201–213. doi: 10.1007/s00382-017-3599-8

Yu, Y., Wang, Y., Cao, L., Tang, R., and Chai, F. (2020). The ocean-atmosphere interaction over a summer upwelling system in the South China sea. *J. Mar. Syst.* 208, 103360. doi: 10.1016/j.jmarsys.2020.103360